

# Air-Ground Cooperation for Cell-Corner Users

Na Deng, Ruiyun Wu, Martin Haenggi, *Fellow, IEEE*, Haichao Wei, Nan Zhao, *Senior Member, IEEE*

**Abstract**—To address the poor performance experienced by cell-corner users located equidistantly to the serving base station (BS) and the nearest interfering BSs, this paper proposes a flexible and general air-ground cooperation scheme based on unmanned aerial vehicles and dynamic BS coordination in the form of BS silencing (BSS) or joint transmission (JT). To show the role of UAV in the cooperation, we define the UAV-to-BS power ratio (UBPR) as a critical parameter to measure whether introducing the UAV can improve the user’s performance. Using stochastic geometry tools, we derive the success probability of the user located at the corner of the Voronoi diagram, called the worst-case user, in Poisson cellular networks. To facilitate the comparison between different modes of cooperation, we further analyze the cooperation gain including the diversity and power gains through the asymptotic outage probability in the high-reliability regime. Furthermore, to reflect the impact of the cooperation scheme on the overall network performance, we analyze the normalized spectral efficiency, which, unlike those adopted in existing works, accounts for the costs of both resource occupancy and data exchange. Numerical results validate the accuracy of our analytical findings and demonstrate the effectiveness of the proposed scheme for cell-corner users.

**Index Terms**—UAV-assisted cellular networks, cell-corner users, air-ground cooperation, success probability, spectral efficiency.

## I. INTRODUCTION

### A. Motivation

As mobile communication continues to advance and diverse applications emerge, user demands for transmission reliability and capacity have grown significantly. For instance, 5G enhanced mobile broadband (eMBB) users seek high transmission rates, while ultra-reliable and low-latency communication (URLLC) users prioritize extremely reliable transmission. However, cell-edge users located relatively far from nearby base stations (BSs) mostly suffer from not only weak desired signal but also severe interference from neighboring BSs in large-scale cellular networks, resulting in low quality of service (QoS) [2]. Consequently, addressing the needs of these cell-edge users has become imperative, as they become the performance bottleneck in the whole network.

Na Deng, Ruiyun Wu and Nan Zhao are with the School of Information and Communication Engineering, Dalian University of Technology, Dalian 116024, China (e-mail: {dengna, zhaonan}@dlut.edu.cn, wury2022@mail.dlut.edu.cn). Martin Haenggi is with the Dept. of Electrical Engineering, University of Notre Dame, Notre Dame 46556, USA (e-mail: mhaenggi@nd.edu). Haichao Wei is with School of Information Science and Technology, Dalian Maritime University, Dalian 116026, China (e-mail: weihachao@dlmu.edu.cn).

Part of this work was presented at the 2024 IEEE Wireless Communications and Networking Conference (WCNC’24) [1]. This work was supported by the National Natural Science Foundation of China under Grant 62371086 and 62201115, the open research fund of State Key Laboratory of Integrated Services Networks under Grant ISN24-10, and the US National Science Foundation under Grant 2007498.

To enhance the performance for cell-edge users, coordinated multipoint (CoMP) is a pivotal solution to the severe inter-cell interference, where BSs communicate with each other over a backhaul link to limit the inter-cell interference (i.e., BS silencing) and transmit together to strengthen the desired signal of a target user (i.e., joint transmission) where possible. While such technique is effective in terms of the improvement of user-perceived performance, it comes at a high cost because the coordinated BSs need to reserve the common idle resources which, as a result, cannot be used to serve their own users. Thus, the overall performance and operating efficiency of the network are bound to be affected. This problem could be solved or alleviated if a new type of access point can be introduced to help improve the performance of cell-corner users without affecting the resource usage and served users in neighboring cells, and accordingly, the unmanned aerial vehicle (UAV)-enabled aerial BS and air-ground cooperation techniques have been emerging very recently [3–5] and bring new opportunities and challenges.

Due to the introduction of mobile access points, a highly flexible and comprehensive air-ground cooperation scheme is needed to deal with various situations while maintaining a high degree of coordination between the ground BSs and UAVs. Furthermore, the existing works mostly focus on general users or cell edge users, and the cell-corner users that usually experience the worst performance have little research attention instead. The particularity of the corner user is that the average received power from the serving BS is equal to that of the equidistant interfering BSs, leading to a fairly low signal-to-interference ratio (SIR), where the interference is an aggregation of the interfering signals from all interferers throughout the network. Meanwhile, although the high maneuverability of the UAV enables it to fly closer to the cell-corner user for better service, the limitations such as power and flight height make the improvement of user performance become uncertain. Therefore, whether the enhancement brought by the UAV can offset the performance degradation caused by the interference is of critical importance for the development of air-ground cooperation in the future but has not been well studied so far. Motivated by this, this paper will investigate the air-ground cooperation for cell-corner users in-depth and try to answer and solve the above questions.

### B. Related Work

The primary causes of poor performance for cell-edge users are the weak desired signal power and the strong interference, both of which can be effectively mitigated by CoMP [6]. As one of the common CoMP techniques, BS silencing (BSS) can effectively alleviate the inter-cell interference and thus improve the communication reliability for users [7, 8]. However, since

BSS does not enhance the desired signal power, the QoS of cell-edge users cannot be substantially improved by using BSS alone due to the weak desired signal strength from the distant serving BS. Thus, another CoMP technique, joint transmission (JT), was adopted in [9–11] to transform the interfering signals from neighboring BSs into the desired signals and combine them to enhance the QoS of cell-edge users. Specifically, in [9], the non-coherent JT scheme of the nearest and the second-nearest BSs was adopted to serve the cell-edge users, and the CoMP activation factor as well as the BS density are jointly optimized to maximize the network energy-spectral efficiency. Since the coordinated BS needs to reserve the spectrum resource for the cell-edge users of other BSs, this will inevitably cause low spectrum efficiency. To attain higher spectrum efficiency, the non-orthogonal multiple access (NOMA) technique is proposed for each BS in [10] to simultaneously serve the cell-center and cell-edge users, where the QoS of cell-edge users are further enhanced via the JT among different BSs. The authors of [11] extended the work in [10] from a two-cell simple scenario to a large-scale cellular network scenario.

Among the cell-edge users, there is a special type named cell-corner users at which the average received power from the serving BS is equal to that from nearby interfering BSs, and accordingly, these users mostly become the network's bottleneck and are in the most need of performance enhancement. The authors in [12] considered the cell-corner users located at the vertexes of the Voronoi diagram in Poisson cellular networks, where each cell-corner user is equidistant to its three closest BSs. Under this setup, the coverage probability and the spectral efficiency were derived using stochastic geometry. To further improve the performance of cell-corner users, JT among the three equidistant BSs was considered in [13] and a tractable framework was proposed to analyze the benefits of BS-JT scheme. In [14], the authors provided a fine-grained analysis on the combination of JT and BSS schemes for cell-corner users, where part of three equidistant neighbor BSs jointly transmit the same data and the other BSs keep silence.

Although CoMP techniques can improve the QoS of cell-corner users, two key issues remain. One is that corner users are more likely to be in a coverage hole than other users since the serving BS(s) are further away statistically, and even JT may not help overcome the resulting weak signal power. The other is that due to the spatiotemporal dynamics of user demands, deploying additional fixed BSs just to improve the performance of cell-corner users is cost-ineffective and inflexible. To solve these issues, UAVs have recently been proposed to complement the terrestrial networks due to its sufficient agility and low deployment cost, serving as temporary aerial BSs for on-demand proximity service [15]. At first, researchers considered the deployment of UAVs in the regions without ground BS coverage such as vast rural areas [16] and disaster-stricken areas [17], and then gradually introduced UAVs to assist BSs in enhancing the quality of service for users in hot-spot [18] or cell-edge regions [19]. The advantage of introducing UAVs lies in that they can be close to their served users and provide better signal quality, but the mutual interference between BSs and UAVs is also

introduced. This is especially serious when two users, each served by a BS and a UAV, are in close proximity. To reduce the mutual interference, the authors in [20] considered UAVs at a fixed exclusion distance from BSs to improve the performance of cell-edge users. However, it is still challenging to meet the highly strict requirements in scenarios like 5G URLLC, especially for cell-corner users who often experience severe interference. This motivates the air-ground cooperation between UAVs and ground BSs to further improve the user-perceived performance. The authors in [21] considered to deploy a UAV in a malfunction area, outside which the ground BSs can still work, and the users therein were served by JT between the UAV and the nearest ground BS. The article of [3] considered that the UAV can fly and hover over the user and cooperatively serve the user with the nearest ground BS, and proposed a generalized Gauss-Poisson process to jointly model the locations of BSs and UAVs for analyzing the benefits of the proposed air-ground JT scheme. In [4], the combination of JT and BSS schemes was proposed for the UAV users, where the nearest ground and aerial BSs provided non-coherent JT and other nearby ground BSs were silenced. Although the above air-ground cooperation schemes show their performance improvement, they assume that merely one nearest ground BS participates in the cooperative transmission and has enough spectrum resource for coordination. Actually, these schemes can hardly be applied to cell-corner users directly. On the one hand, due to the three equidistant nearest BSs, the received signal strength from the serving BS might be comparative to that from other neighbor (interfering) BSs. Thus, the performance improvement might be limited by many factors such as the UAV's height, signal propagation environment, the distance to the nearest BSs, coordination manner, etc. On the other hand, since neighbor BSs are required to reserve extra resources for the coordination, whether they can participate in the coordination depends on their user loads and coordination costs. To our best knowledge, it has been unexplored on how to effectively utilize the three equidistant nearest BSs and UAV to enhance the performance of cell-corner users while balancing the above complex factors well.

### C. Contributions

In this paper, we propose a flexible and general air-ground cooperation scheme to enhance the performance of cell-corner users, which includes various modes of cooperation such as BSS- and JT-based cooperation with and without UAV assistance. The flexibility is embodied in two aspects: one is that not all the corner users have a UAV hovering over them to provide air-ground cooperation; the other is that the scheme involves different levels of cooperation, from single UAV or BS (without cooperation) to one UAV plus three equidistant BSs (the highest level of cooperation). On the one hand, such design is closer to real networks considering the high maneuverability of the UAV as well as the willingness of BSs to provide cooperation; on the other hand, different from the existing schemes with a fixed mode and level of cooperation, our scheme is more general with dynamic cooperation levels that improve the user-perceived performance while minimizing the impact on the quality of service in the neighboring cells.

To fully evaluate the performance benefits brought by this scheme, we model the locations of BSs by a Poisson point process. The locations of cell-corner users are the vertices of the Poisson-Voronoi diagram, also named the worst-case users. To reflect the role of UAV in the cooperation, we define the UAV-to-BS power ratio (UBPR) as a critical parameter to measure whether adding a UAV can improve the user's performance. Under the proposed air-ground cooperation scheme, we derive the success probability and its asymptotic behavior for the worst-case user with the aid of stochastic geometry tools. It turns out that for different types of cooperation, the success probability has a consistent form of its asymptotic behavior which can be used to characterize the user-perceived performance in the high-reliability regime. On this basis, we introduce and analyze the normalized spectral efficiency (NSE) to reflect the cost of different coordinations taking the resource occupancy and data exchange overhead into account, where the latter is rarely considered in the existing works. Numerical results demonstrate the accuracy of the derived expression and highlight the superior performance of the cooperations with UAV assistance relative to those without UAV assistance and the dynamic number of coordinated points in terms of success probability and NSE.

## II. SYSTEM MODEL

### A. Network Model

We consider a UAV-assisted cellular downlink network, where the locations of BSs follow a homogeneous PPP  $\Phi_b = \{x_1, x_2, \dots\}$  of density  $\lambda$  in the Euclidean plane  $\mathbb{R}^2$ . Each BS has a transmit power of  $\mu_b$  and is equipped with an omnidirectional antenna. We focus on the worst-case users, which are located at the Voronoi corners and have three equidistant BSs. When randomly choosing one as the serving BS, these users experience severe interference from the two other equidistant BSs and can be regarded as the worst-case users from a geometric point of view [12, 22]. To enhance the QoS of these worst-case users, some UAVs are assumed to hover over the vertices of the Voronoi diagram at a height of  $h$  to serve as aerial BSs and each vertex has a UAV with probability  $p$  to control the UAV deployment cost. According to [23, Tier 3], the projection locations of UAVs are obtained via retaining the Voronoi vertices with probability  $p$ , which results in a stationary point process  $\Phi_u$  with density  $2p\lambda$ . Each UAV has a transmit power of  $\mu_u$  and is equipped with a directional antenna array to provide downward beam coverage. A common sectorized model in [24] is used to capture directional transmission, expressed by

$$G(\phi) = \begin{cases} G_m & \text{if } |\phi| \leq \psi_m \\ G_s & \text{otherwise,} \end{cases} \quad (1)$$

where  $\phi$  is the angle of the transmit signal off the baseline downward direction,  $G_m$  and  $G_s$  denote the antenna gains for the main and side lobes, respectively, and  $\psi_m$  is the half of the half-power beamwidth (HPBW). Therefore, the main lobe beam of UAV  $y$  (its projection location at  $y$ ) is a coverage disk centered at  $y$  with radius  $R_m = h \tan \psi_m$ . Furthermore, the ground BSs and the UAVs share the spectrum resources.

### B. Channel Model

For the worst-case users, the desired signal comes from a BS via a terrestrial channel or a UAV via an air-to-ground channel. For the terrestrial channel, the propagation condition is non-line-of-sight (NLOS), and the bounded path loss model  $\ell_b(r) = \max\{r, d_0\}^{-\alpha_N}$  is adopted with the NLOS path loss exponent  $\alpha_N$ , the propagation distance  $r$  and the bounded parameter  $d_0$  reflecting the reference distance. Rayleigh fading is assumed to capture the scattering effect of the NLOS channel, and the power fading coefficient follows an exponential distribution. For the air-to-ground channel, there are both line-of-sight (LOS) and NLOS propagation conditions, and we adopt a common probabilistic model in [25], where the LOS probability of an air-to-ground channel with the horizontal distance  $r$  and the UAV height  $h$  is

$$P_L(r) = \frac{1}{1 + \nu \exp(-\kappa(\frac{180}{\pi} \arctan(h/r) - \nu))}, \quad (2)$$

where  $\nu$  and  $\kappa$  are constants that allow an adjustment to different propagation environments. The NLOS probability is  $P_N(r) = 1 - P_L(r)$ . Let  $\alpha_L$  denote the path loss exponent for the LOS channel, where  $2 < \alpha_L < \alpha_N$ , and the random path loss function of the air-to-ground channel is

$$\ell_u(r) = \begin{cases} (r^2 + h^2)^{-\alpha_L/2} & \text{w.p. } P_L(r) \\ (r^2 + h^2)^{-\alpha_N/2} & \text{w.p. } P_N(r). \end{cases} \quad (3)$$

Nakagami fading is adopted to model the small-scale fading in the LOS channel, and thus the power fading coefficient follows a gamma distribution  $\text{gamma}(m_L, 1/m_L)$  with the integer  $m_L > 1$ . Furthermore, we assume that the power fading coefficients are mutually independent and also independent of  $\Phi_b$  and  $\Phi_u$ . Due to the flexibility of UAVs, we assume that the desired signal from the UAV experiences a LOS propagation, and thus its path loss is  $h^{-\alpha_L}$  with the power fading coefficient following  $\text{gamma}(m_L, 1/m_L)$ .

### C. Air-ground Cooperation Scheme

The extent to which UAV-assisted cellular networks can improve the performance of the worst-case users is affected and limited by various factors. Although the desired signal strength will definitely be enhanced with the assistance of UAVs, the degree of such enhancement mostly depends on the UAV's height, which is constrained by the realistic environments and regulations of the government and industrial association [15]. That is to say, the desired signal strength cannot be increased at will. However, the worst-case users often experience quite severe interference from their surrounding BSs, especially from the equidistant interfering BSs. Therefore, whether the enhancement by the assistance of UAVs can offset the performance degradation caused by the interference is of great importance in determining whether it is necessary to introduce UAVs to cellular networks considering the associated additional costs. To fully address this critical issue, we formally define a critical parameter  $\rho$ , named UAV-to-BS power ratio (UBPR), as follows.

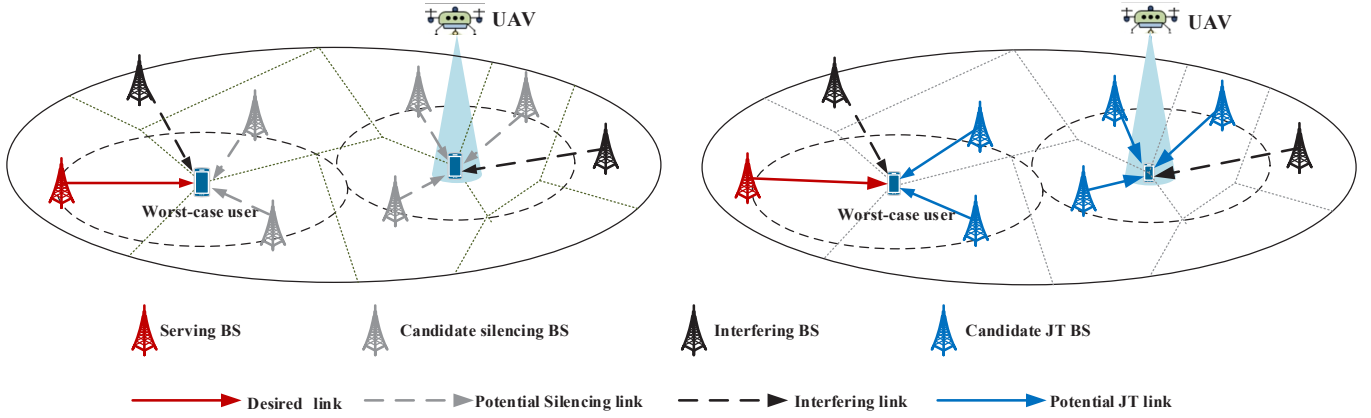


Fig. 1. An illustration of the proposed air-ground cooperation scheme, including the BSS-based and JT-based cooperations with and without UAV assistance.

**Definition 1.** The UBPR is defined as the ratio of the average powers received from the desired UAV to BS, given by

$$\rho \triangleq \mu_u G_m h^{-\alpha_L} / (\mu_b \ell_b(\mathbb{E}D)), \quad (4)$$

where  $D$  is the distance from the worst-case user to its three nearest equidistant BSs.

It is expected that there would be three cases:

- 1) When  $\rho \gg 1$ , the UAV contributes a lot to the desired signal strength, and the BSs are of limited help.
- 2) When  $\rho \approx 1$ , the UAV contributes about the same as the serving BS.
- 3) When  $\rho \ll 1$ , the role of the UAV is negligible.

For case 1), having the equidistant nearest BSs not interfere is almost as good as having them cooperate with the UAV. For case 2), it is better to let the UAV to transmit together with one or more BSs than separately, i.e., to establish an air-ground JT. As for the last case, it would be unnecessary to add a UAV.

Motivated by the above discussions, we propose a flexible and general air-ground cooperation scheme to enhance the performance of the worst-case users, where the three equidistant nearest BSs and the possible hovering UAV naturally constitute a potential cooperation set to provide service in different collaborative manners including the BSS and JT, shown in Fig. 1. Due to the stationarity of  $\Phi_b$  and  $\Phi_u$ , we take the typical worst-case user located at the origin as an example to specify the proposed air-ground cooperation scheme. Specifically, let  $\mathcal{V} \triangleq \arg \min_{x \in \Phi_b} \|x\| = \{x_1, x_2, x_3\}$

be the set of the three equidistant closest BSs. In the case without a UAV hovering over the worst-case user, a BS in  $\mathcal{V}$  is randomly chosen to be the primary serving BS, say  $x_1$ , and the other two equidistant BSs could participate in the cooperation according to their traffic loads. As a result, the user can be served by a cooperation set  $\mathcal{W} \subseteq \mathcal{V}$  and  $\mathcal{W} \supset \{x_1\}$ , and the number of coordinated BSs is denoted by  $N = \#\mathcal{W} \in \{1, 2, 3\}$ . While in the case with a UAV hovering over the worst-case user, the UAV becomes the primary serving aerial BS, and the three equidistant BSs could selectively participate in the cooperation. Thus, the user can be served by the UAV collaboratively with the BSs in the cooperation set  $\mathcal{W} \subseteq \mathcal{V}$ , and the number of coordinated BSs is

denoted by  $N = \#\mathcal{W} \in \{0, 1, 2, 3\}$ . Furthermore, we consider two collaborative manners in current 4G/5G cellular systems: one is the non-coherent JT, and the other is the BSS according to the burden on X2/Xn interface among BSs.

#### D. SIR Analysis

In the following, we establish the SIR expressions under different collaborative manners.

1) *Non-coherent JT*: Under this collaborative manner, the signal amplitudes on the same resource element add up from different desired sources, and the aggregated signal power includes the square of the signal amplitude from each source and the cross-product terms from different sources. Due to the timing offset, each cross-product term varies quickly within the coherence bandwidth, and the average over these power variations is proposed to obtain the average SINR experienced on coherent subcarriers in [26]. Consequently, the desired signal power is approximated as the accumulation of the signal powers from different sources<sup>1</sup>. Therefore, the received signal-to-interference ratio (SIR) for the case without UAV assistance is

$$\text{SIR}_{\text{JTG}} = \frac{\mu_b \ell_b(D) \sum_{x \in \mathcal{W}} g_x}{I_{nc} + I_b + I_u}, \quad (5)$$

where  $D = \|x_1\| = \|x_2\| = \|x_3\|$ ,  $I_{nc}$  is the interference from  $3-N$  non-cooperative BSs in  $\mathcal{V} \setminus \mathcal{W}$ ,  $I_b$  is the interference from other interfering BSs in  $\Phi_b \setminus \mathcal{V}$ , and  $I_u$  is the interference from UAVs in  $\Phi_u$ . The three types of interference are expressed, respectively, as

$$I_{nc} = \mu_b \sum_{x \in \mathcal{V} \setminus \mathcal{W}} g_x \ell_b(D), \quad (6)$$

$$I_b = \mu_b \sum_{x \in \Phi_b \setminus \mathcal{V}} g_x \ell_b(\|x\|), \quad (7)$$

$$I_u = \mu_u \sum_{x \in \Phi_u} g_x G_x \ell_u(\|x\|), \quad (8)$$

<sup>1</sup>The detailed transmission and reception procedure in non-coherent JT as well as the corresponding mathematical derivations can be found in Appendix A in [26].

where  $g_x$  denotes the power fading coefficient from BS  $x \in \Phi_b$  or UAV  $x \in \Phi_u$ , and  $G_x$  is the antenna array gain from UAV  $x$  following (1). For the air-ground JT (i.e., with the UAV assistance), the received SIR is expressed as

$$\text{SIR}_{\text{JTAG}} = \frac{\mu_u G_m h^{-\alpha_L} g_{u_0} + \mu_b \sum_{x \in \mathcal{W}} \ell_b(D) g_x}{I_{\text{nc}} + I_b + I_u}, \quad (9)$$

where  $I_{\text{nc}}$  and  $I_b$  are given in (6) and (7), respectively, and

$$I_u = \mu_u \sum_{x \in \Phi_u \setminus u_0} g_x G_x \ell_u(\|x\|). \quad (10)$$

2) *BSS*: Under this collaborative manner, the BSs participating in the cooperation silence their transmissions on the resource blocks allocated to the worst-case user so as to avoid causing interference. For the case without UAV assistance, the received SIR for the typical worst-case user is given by

$$\text{SIR}_{\text{SG}} = \frac{\mu_b \ell_b(D) g_{x_1}}{I_{\text{nc}} + I_b + I_u}, \quad (11)$$

where  $I_{\text{nc}}$ ,  $I_b$ , and  $I_u$  are given in (6), (7), and (8), respectively. For the case with UAV assistance, the received SIR is given by

$$\text{SIR}_{\text{SAG}} = \frac{\mu_u h^{-\alpha_L} G_m g_{u_0}}{I_{\text{nc}} + I_b + I_u}, \quad (12)$$

where  $I_{\text{nc}}$ ,  $I_b$ , and  $I_u$  are given in (6), (7), and (10), respectively.

Note that from the SIR expressions, it can be obviously seen that the performance enhancement achieved by JT is more significant than BSS. However, the former in practice requires data sharing among the coordinated points which brings severe signaling and data burdens to the backhaul links, while the latter does not have such problem and is easy to implement. Since both schemes have their applicable scenes, we integrate them into a general air-ground cooperation scheme and investigate its performance in different aspects.

### III. PERFORMANCE ANALYSIS

In this section, we use the success probability and normalized spectral efficiency as the criteria to evaluate the performance of the proposed air-ground cooperation scheme including JT-based and BSS-based cooperations with and without UAV assistance.

#### A. Auxiliary Results

This part gives some auxiliary results that are essential for the following analysis, including the distance distribution, the Laplace transform of different types of interference and their derivatives, as well as the desired signal power distribution in different collaborative manners.

Firstly, the probability density function (PDF) of  $D$  for the typical worst-case user is given by [12]

$$f_D(t) = 2(\lambda\pi)^2 t^3 \exp(-\lambda\pi t^2), \quad t \geq 0. \quad (13)$$

Then the expectation of this distance can be obtained as

$$\mathbb{E}D = \int_0^\infty 2(\lambda\pi)^2 t^4 \exp(-\lambda\pi t^2) dt = \frac{3}{4\sqrt{\lambda}}. \quad (14)$$

It is worth noting that this average serving distance of the worst-case user is 50% larger than that of the typical (overall) user  $\frac{1}{2\sqrt{\lambda}}$  in Poisson cellular networks [27].

Subsequently, we present the key intermediate results concerning the conditional Laplace transform of the interference given  $D = t$  and its derivatives in the following lemmas. For notational convenience, we define  $m_N \triangleq 1$ ,

$$\Psi_i(s, r, x) \triangleq 1 - \left(1 + \frac{s\mu_u x}{m_i(r^2 + h^2)^{\alpha_i/2}}\right)^{-m_i},$$

$$\mathcal{G}(r) \triangleq G_m \mathbf{1}(r \leq R_m) + G_s \mathbf{1}(r > R_m), \quad (15)$$

where  $\mathbf{1}(\cdot)$  is the indicator function.

**Lemma 1.** *Given  $D = t$ , the Laplace transforms of the three types of interference in the two collaborative manners are expressed by*

$$\mathcal{L}_{I_{\text{nc}}}(s, t) = (1 + \mu_b s \ell_b(t))^{N-3}$$

$$\mathcal{L}_{I_b}(s, t) = \exp\left(-2\pi\lambda \int_t^\infty \frac{r}{1 + \mu_b^{-1} s^{-1} \ell_b^{-1}(r)} dr\right),$$

$$\mathcal{L}_{I_u}(s) \approx \exp\left(-4p\pi\lambda \sum_{i \in \{L, N\}} \int_0^\infty \Psi_i(s, r, \mathcal{G}(r)) P_i(r) r dr\right) \quad (16)$$

*Proof: See Appendix A.*

The aggregated interference is  $I = I_{\text{nc}} + I_b + I_u$  and the following lemma gives the derivatives of the Laplace transform.

**Lemma 2.** *Let  $\mathcal{L}_{I_{\text{re}}}(s, t) \triangleq \mathcal{L}_{I_b}(s, t) \mathcal{L}_{I_u}(s)$  and*

$$\eta(s, t) \triangleq -2\pi\lambda \int_t^\infty \left(1 - \frac{1}{1 + \mu_b s \ell_b(r)}\right) r dr$$

$$-4\pi p\lambda \sum_{i \in \{L, N\}} \int_0^\infty \Psi_i(s, r, \mathcal{G}(r)) P_i(r) r dr. \quad (17)$$

*The  $n$ -th derivative of  $\mathcal{L}_I(s, t) = \mathcal{L}_{I_{\text{nc}}}(s, t) \mathcal{L}_{I_b}(s, t) \mathcal{L}_{I_u}(s)$  w.r.t.  $s$  is given by*

$$\mathcal{L}_I^{(n)}(s, t) = \sum_{k=0}^n \binom{n}{k} \mathcal{L}_{I_{\text{nc}}}^{(n-k)}(s, t) \mathcal{L}_{I_{\text{re}}}^{(k)}(s, t), \quad (18)$$

where

$$\mathcal{L}_{I_{\text{nc}}}^{(n)}(s, t) = \frac{\Gamma(n+3-N)(-\mu_b \ell_b(t))^n}{\Gamma(3-N)(1 + \mu_b s \ell_b(t))^{3-N+n}}, \quad n \geq 0, \quad (19)$$

$$\mathcal{L}_{I_{\text{re}}}^{(k)}(s, t) = \sum_{l=0}^{k-1} \binom{k-1}{l} \eta^{(k-l)}(s, t) \mathcal{L}_{I_{\text{re}}}^{(l)}(s, t), \quad k > 0, \quad (20)$$

$$\eta^{(k)}(s, t) = (-1)^k 2\pi\lambda \left[ \mu_b^k \int_t^\infty \frac{\Gamma(1+k) \ell_b^k(r) r dr}{(1 + \mu_b s \ell_b(r))^{k+1}} + 2p \right.$$

$$\left. \times \sum_{i \in \{L, N\}} \frac{\Gamma(m_i + k) \mu_u^k}{\Gamma(m_i) m_i^k} \int_0^\infty \frac{\mathcal{G}^k(r) (r^2 + h^2)^{-\frac{k\alpha_i}{2}} P_i(r) r}{(1 + \frac{s\mathcal{G}(r)\mu_u}{m_i(r^2 + h^2)^{\alpha_i/2}})^{m_i+k}} dr \right] \quad (21)$$

*Proof: See Appendix B.*

Next, we provide the conditional probability distribution of the desired signal power, denoted by  $S$ , received by the typical worst-case user given  $D = t$ . If BSS is adopted,  $S$  is

merely from the serving BS (or UAV) and follows the gamma distribution as

$$S = \mu_b \ell_b(D) g_{x_1} \sim \text{gamma}(K=1, \theta = \mu_b \ell_b(t)),$$

$$S = \mu_u G_m h^{-\alpha_L} g_{u_0} \sim \text{gamma}(K=m_L, \theta = \frac{\mu_u G_m h^{-\alpha_L}}{m_L}), \quad (22)$$

for the case without and with a hovering UAV, respectively. If non-coherent JT is adopted,  $S$  is a sum of two gamma variables, where one is from the serving BS (or UAV), as in (22), and the other is the aggregated signal power from the cooperative BSs in  $\mathcal{W}$ , expressed by

$$\mu_b \sum_{x \in \mathcal{W}} \ell_b(D) g_x \sim \text{gamma}(K=N, \theta = \mu_b \ell_b(t)). \quad (23)$$

Therefore, in the case without a hovering UAV, we have

$$S \sim \text{gamma}(K=N, \theta = \mu_b \ell_b(t)), \quad (24)$$

while in the case with a hovering UAV, due to different scale parameters of the two gamma variables, the exact probability distribution of  $S$  is in a complex form [28], which challenges the derivation of the success probability. As a result, we adopt the second-order moment matching method to introduce a new gamma random variable  $J \sim \text{gamma}(K, \theta)$  to approximate  $S$ , which has only a small margin of error [29]. For  $J$ , the parameters  $K, \theta$  depend on the distance  $D$ , and given  $D = t$ , they are expressed as

$$K(t) = \frac{(\mu_u G_m h^{-\alpha_L} + N \mu_b \ell_b(t))^2}{(\mu_u G_m h^{-\alpha_L})^2 / m_L + N (\mu_b \ell_b(t))^2}, \quad (25)$$

$$\theta(t) = \frac{(\mu_u G_m h^{-\alpha_L})^2 / m_L + N (\mu_b \ell_b(t))^2}{\mu_u G_m h^{-\alpha_L} + N \mu_b \ell_b(t)}. \quad (26)$$

It is obtained that  $\mathbb{E}[J|D=t] = \mu_u G_m h^{-\alpha_L} + N \mu_b \ell_b(t)$  is the mean received power from all cooperators and that the variance  $\text{var}(J|D=t) = (1/m_L)(\mu_u G_m h^{-\alpha_L})^2 + N(\mu_b \ell_b(t))^2$  is the squared mean powers scaled by  $1/m_L$  and  $N$ , respectively. Tab. I summarizes the shape parameter  $K(t)$  and scale parameter  $\theta(t)$  for the conditional gamma distributions of the desired signal power given  $D = t$  in different cases.

### B. Success Probability

The success probability is defined as the complementary cumulative distribution function (CCDF) of the SIR, given by

$$P_s(T) \triangleq \mathbb{P}(\text{SIR} > T), \quad (27)$$

where  $T$  denotes the SIR threshold. After obtaining the conditional probability distribution of the desired signal power  $S$  and the conditional Laplace transform of the aggregated interference  $\mathcal{L}_I(s, t)$ , the success probability of the worst-case user can be obtained. We first focus on the cases with integer shape parameter of the gamma variable  $S$ .

**Theorem 1.** *The success probability of the typical worst-case user is approximated as*

$$P_s(T) \approx \sum_{n=1}^K \binom{K}{n} (-1)^{n+1} \int_0^\infty f_D(t) \mathcal{L}_I\left(\frac{n\xi T}{\theta(t)}, t\right) dt, \quad (28)$$

where  $\xi = (\Gamma(1+K))^{-1/K}$ ,  $K$  and  $\theta(t)$  are found in Tab. I for the cases of BSS with/without UAV assistance and JT without UAV assistance, respectively.

*Proof:* With the PDF of  $D$ , the Laplace transform of  $I(t)$  and the probability distribution of  $S$ , the success probability is given by

$$\begin{aligned} P_s(T) &= \mathbb{P}(S > TI) \\ &= \int_0^\infty \mathbb{P}(S > TI(t)) f_D(t) dt \\ &= \int_0^\infty \mathbb{E}\left[\tilde{\Gamma}\left(K, \frac{TI(t)}{\theta(t)}\right)\right] f_D(t) dt \\ &\stackrel{(a)}{\leq} \int_0^\infty \mathbb{E}\left[1 - \left(1 - \exp\left(-\frac{\xi TI(t)}{\theta(t)}\right)\right)^K\right] f_D(t) dt \\ &\stackrel{(b)}{=} \int_0^\infty \mathbb{E}\left[\sum_{n=1}^K \binom{K}{n} (-1)^{n+1} \exp\left(-\frac{n\xi TI(t)}{\theta(t)}\right)\right] f_D(t) dt \\ &= \int_0^\infty f_D(t) \sum_{n=1}^K \binom{K}{n} (-1)^{n+1} \mathcal{L}_I\left(\frac{n\xi T}{\theta(t)}, t\right) dt, \quad (29) \end{aligned}$$

where step (a) follows from the tight upper bound for the normalized upper incomplete gamma function  $\tilde{\Gamma}(\cdot)$  in [30], given by

$$\begin{aligned} \mathbb{P}(S > v) &= \tilde{\Gamma}(K, v/\theta(t)) \\ &\leq 1 - \left(1 - \exp\left(-(\Gamma(1+K))^{-\frac{1}{K}} \frac{v}{\theta(t)}\right)\right)^K, \end{aligned}$$

and step (b) follows from the binomial theorem. ■

Then we focus on the case with non-integer shape parameter of the gamma variable  $S$ , i.e., non-coherent JT with UAV assistance.

**Theorem 2.** *The success probability of the typical worst-case user for the case of JT with UAV assistance is approximated as*

$$P_s(T) \approx \int_0^\infty \sum_{n=1}^\infty \binom{K(t)}{n} (-1)^{n+1} f_D(t) \mathcal{L}_I\left(\frac{n\xi(t)T}{\theta(t)}, t\right) dt, \quad (30)$$

where  $\xi(t) = (\Gamma(1+K(t)))^{-1/K(t)}$ , and  $K(t)$  and  $\theta(t)$  are found in Tab. I.

*Proof:* Similar to the proof of Thm. 1, we have

$$\begin{aligned} P_s(T) &= \mathbb{P}(S > TI) \\ &\approx \mathbb{P}(J > TI) \\ &\leq \int_0^\infty \mathbb{E}\left[1 - \left(1 - \exp\left(-\frac{\xi(t)TI(t)}{\theta(t)}\right)\right)^{K(t)}\right] f_D(t) dt \\ &\stackrel{(a)}{=} \int_0^\infty \mathbb{E}\left[\sum_{n=1}^\infty \binom{K(t)}{n} (-1)^{n+1} \exp\left(-\frac{n\xi(t)TI(t)}{\theta(t)}\right)\right] f_D(t) dt \\ &= \int_0^\infty f_D(t) \sum_{n=1}^\infty \binom{K(t)}{n} (-1)^{n+1} \mathcal{L}_I\left(\frac{n\xi(t)T}{\theta(t)}, t\right) dt, \quad (31) \end{aligned}$$

where step (a) follows from the generalized binomial theorem. ■

To simplify the computation in Thm. 2, we further use the approximation  $\mathbb{E}K(D) \approx K(\mathbb{E}D)$  and obtain a simplified expression of the success probability in the following corollary.

TABLE I. The shape and scale parameters in different cases.

Case	$K$ or $K(t)$	$\theta(t)$	Diversity Gain $d$	$\varrho$ in Thm. 3
BSS without UAV assistance	1	$\mu_b \ell_b(t)$	1	(41)
BSS with UAV assistance	$m_L$	$\frac{\mu_u G_m h^{-\alpha_L}}{m_L}$	$m_L$	(42)
JT without UAV assistance	$N$	$\mu_b \ell_b(t)$	$N$	(43)
JT with UAV assistance	(25)	(26)	$N + m_L$	(44)

**Corollary 1.** *Letting*

$$\bar{K} \triangleq \int_0^\infty \frac{(\mu_u G_m h^{-\alpha_L} + N \mu_b \ell_b(t))^2}{(\mu_u G_m h^{-\alpha_L})^2 / m_L + N (\mu_b \ell_b(t))^2} f_D(t) dt, \quad (32)$$

the success probability of the typical worst-case user for the case of JT with UAV assistance is approximated as

$$P_s(T) \approx \sum_{n=1}^{\infty} \binom{\bar{K}}{n} (-1)^{n+1} \int_0^\infty f_D(t) \mathcal{L}_I\left(\frac{n \bar{\xi} T}{\theta(t)}, t\right) dt, \quad (33)$$

where  $\bar{\xi} = (\Gamma(1 + \bar{K}))^{-1/\bar{K}}$ , and  $\theta(t)$  is found in Tab. I.

*Proof:* Similar to the proof of Thm. 2, we have

$$\begin{aligned} P_s(T) &\leq \int_0^\infty \mathbb{E} \left[ 1 - \left( 1 - \exp\left(-\frac{\xi(t) T I(t)}{\theta(t)}\right) \right)^{K(t)} \right] f_D(t) dt \\ &\stackrel{(a)}{\approx} \int_0^\infty \mathbb{E} \left[ 1 - \left( 1 - \exp\left(-\frac{\bar{\xi} T I(t)}{\theta(t)}\right) \right)^{\bar{K}} \right] f_D(t) dt \\ &= \int_0^\infty \mathbb{E} \left[ \sum_{n=1}^{\infty} \binom{\bar{K}}{n} (-1)^{n+1} \exp\left(-\frac{n \bar{\xi} T I(t)}{\theta(t)}\right) \right] f_D(t) dt \\ &= \int_0^\infty f_D(t) \sum_{n=1}^{\infty} \binom{\bar{K}}{n} (-1)^{n+1} \mathcal{L}_I\left(\frac{n \bar{\xi} T}{\theta(t)}, t\right) dt, \quad (34) \end{aligned}$$

where step (a) is obtained via approximating  $K(t)$  with its average  $\bar{K} = \int_0^\infty K(t) f_D(t) dt$ . ■

In Thm. 2 and Cor. 1, the infinite sum results in a high computational complexity since  $K(t)$  and  $\bar{K}$  are not integers. To obtain a finite sum, we further propose an approximation for the success probability via obtaining an upper integer bound of the shape parameter  $K$ .

**Corollary 2.** *Letting  $\tilde{K} = m_L + N$ ,  $\tilde{\xi} = (\Gamma(1 + \tilde{K}))^{-1/\tilde{K}}$  and  $\tilde{\theta}(t) = \frac{1}{\tilde{K}} (\mu_u G_m h^{-\alpha_L} + N \mu_b \ell_b(t))$ , the success probability for the case of JT with UAV assistance has the approximation*

$$P_s(T) \approx \sum_{n=1}^{\tilde{K}} \binom{\tilde{K}}{n} (-1)^{n+1} \int_0^\infty f_D(t) \mathcal{L}_I\left(\frac{n \tilde{\xi} T}{\tilde{\theta}(t)}, t\right) dt. \quad (35)$$

*Proof:* Letting  $\mathbf{a}$  be a column vector with the  $i$ -th element  $a_i = 1$  for  $i = 1, \dots, N + m_L$  and  $\mathbf{b}$  be a column vector with  $b_i = \frac{\mu_u G_m h^{-\alpha_L}}{m_L}$ ,  $i = 1, \dots, m_L$  and  $b_i = \mu_b \ell_b(t)$ ,  $i = m_L + 1, \dots, m_L + N$ , we rewrite the numerator of  $K(t)$  in (25) in the inner product form of  $(\mathbf{a}^T \mathbf{b})^2$ . According to the Cauchy-Schwarz inequality, we have

$$K(t) \leq \frac{\left( \sum_{i=1}^{N+m_L} a_i^2 \right) \times \left( \sum_{i=1}^{N+m_L} b_i^2 \right)}{\frac{(\mu_u G_m h^{-\alpha_L})^2}{m_L} + N (\mu_b \ell_b(t))^2}$$

$$\begin{aligned} &= \frac{(m_L + N) \left[ m_L \left( \frac{\mu_u G_m h^{-\alpha_L}}{m_L} \right)^2 + N (\mu_b \ell_b(t))^2 \right]}{\frac{(\mu_u G_m h^{-\alpha_L})^2}{m_L} + N (\mu_b \ell_b(t))^2} \\ &= m_L + N. \quad (36) \end{aligned}$$

Via matching the first-order moment and using a gamma random variable  $\tilde{J} \sim \text{gamma}(m_L + N, \tilde{\theta}(t))$  to approximate  $S$ , we can obtain the final results similar to Theorem 1. ■

### C. Cooperation Gain

To characterize the performance enhancement brought by different modes of cooperation clearly, we analyze the diversity gain and power gain for the worst-case user in this part. Specifically, the diversity gain is defined as the decay rate to zero of the outage probability  $1 - P_s(T)$  for the high-reliability regime, expressed by [7]

$$d \triangleq \lim_{T \rightarrow 0} \frac{\log(1 - P_s(T))}{\log T}, \quad (37)$$

which implies that the outage probability has the asymptotic form

$$1 - P_s(T) \sim \varrho T^d, \quad T \rightarrow 0, \quad (38)$$

where  $\varrho$  is a constant independent of the SIR threshold  $T$ . The power gain PG is defined as the asymptotic SIR gain in the high-reliability regime that can be achieved by a certain type of cooperation relative to the benchmark (i.e., without cooperation). Mathematically [13]

$$\text{PG} \triangleq \frac{\left( \lim_{T \rightarrow 0} \frac{T^{d_{\text{coop}}}}{1 - P_{s,\text{coop}}(T)} \right)^{1/d_{\text{coop}}}}{\left( \lim_{T \rightarrow 0} \frac{T^{d_{\text{bench}}}}{1 - P_{s,\text{bench}}(T)} \right)^{1/d_{\text{bench}}}}, \quad (39)$$

where  $P_{s,\text{coop}}(T)$  and  $P_{s,\text{bench}}(T)$  are the success probability of a certain type of cooperation and the benchmark, and  $d_{\text{coop}}$  and  $d_{\text{bench}}$  are the corresponding diversity gains, respectively. Substituting (38) into (39), the power gain can be obtained by

$$\text{PG} = \varrho_{\text{coop}}^{-1/d_{\text{coop}}} / \varrho_{\text{bench}}^{-1/d_{\text{bench}}}. \quad (40)$$

In the following, we provide the diversity gain and constant term  $\varrho$  for different modes of cooperation.

**Theorem 3.** *The asymptotic behavior of the outage probability in different modes of cooperation has a consistent form in (38). For the BSS without UAV assistance, the diversity gain is 1, and*

$$\begin{aligned} \varrho_{\text{SG}} &= 3 - N + \mathcal{P} \\ &+ \frac{4p\pi\lambda_b\mu_u\mathcal{Q}}{\mu_b} \sum_{i \in \{L, N\}} \int_0^\infty \frac{\mathcal{G}(r) P_i(r) r}{(r^2 + h^2)^{\alpha_i/2}} dr, \quad (41) \end{aligned}$$

TABLE II. Symbols and descriptions.

Symbol	Description	Default value
$\Phi_b, \lambda$	The BS point process and its density	$\lambda = 1 \times 10^{-4} \text{ m}^{-2}$
$p$	The probability of a Voronoi corner having a UAV over it	0.5
$\Phi_u, \lambda_u$	The horizontal point process of the UAVs and its density	$\lambda_u = 2p\lambda$
$\mu_b, \mu_u$	The transmit power of the BS and UAV	$\mu_b = 40 \text{ W}, \mu_u = 0.5 \text{ W}$
$D$	The distance between the worst-case user and its three nearest equidistant BSs	N/A
$h$	The hovering altitude of the UAVs	150 m
$G_m, G_s, \psi_m$	The antenna gains of the main lobe and side lobe, and the half HPBW	10, 0.1, $\frac{\pi}{12}$
$\alpha_L, \alpha_N$	The path loss exponents of the LOS and NLOS links	2.5, 4
$d_0$	The parameter of the bounded path loss model	1 m
$m_L, m_N$	The fading parameters of the LOS and NLOS links	3, 1
$\nu, \kappa$	The parameters in the LOS probability model	11.95, 0.136 [31]
$N$	The number of coordinated BSs	N/A
$\varpi$	The parameter in characterizing the cost of data exchange in JT	0.2

where

$$\mathcal{P} = \frac{2\Gamma(3, \pi\lambda_b d_0^2) + \pi\lambda_b \alpha_N d_0^2 \gamma(2, \pi\lambda_b d_0^2)}{\alpha_N - 2} - \gamma(3, \pi\lambda_b d_0^2),$$

$$\mathcal{Q} = d_0^{\alpha_N} \gamma(2, \lambda_b \pi d_0^2) + (\lambda_b \pi)^{-\frac{\alpha_N}{2}} \Gamma\left(\frac{\alpha_N}{2} + 2, \lambda_b \pi d_0^2\right).$$

For the BSS with UAV assistance, the diversity gain is  $m_L$ , and

$$\varrho_{\text{SAG}} = \int_0^\infty \frac{(-1)^{m_L} \mathcal{L}_I^{(m_L)}(s, t)|_{s=0} f_D(t) dt}{\Gamma(m_L + 1) \left(\frac{\mu_u G_m h^{-\alpha_L}}{m_L}\right)^{m_L}}. \quad (42)$$

For the JT without UAV assistance, the diversity gain is  $N$ , and

$$\varrho_{\text{JTG}} = \int_0^\infty \frac{(-1)^{1+N} \mathcal{L}_I^{(1+N)}(s, t)|_{s=0} f_D(t) dt}{\Gamma(N + 2) (\mu_b \ell_b(t))^{N+1}}. \quad (43)$$

For the JT with UAV assistance, the diversity gain is  $N + m_L$ , and

$$\varrho_{\text{JTAG}} = \int_0^\infty \frac{(-1)^{m_L + N} \mathcal{L}_I^{(m_L + N)}(s, t)|_{s=0} f_D(t) dt}{\Gamma(m_L + N + 1) \left(\frac{\mu_u G_m h^{-\alpha_L}}{m_L}\right)^{m_L} (\mu_b \ell_b(t))^N}. \quad (44)$$

In (42)-(44), the  $n$ -th derivative of  $\mathcal{L}_I(s, t)$  w.r.t.  $s$  at  $s = 0$  is given by

$$\mathcal{L}_I^{(n)}(s, t)|_{s=0} = \sum_{k=0}^n \binom{n}{k} \frac{\Gamma(n - k + 3 - N) \tilde{\mathcal{L}}_{\text{Ire}}^{(k)}(t)}{\Gamma(3 - N) (-\mu_b \ell_b(t))^{k-n}}, \quad (45)$$

where  $\tilde{\mathcal{L}}_{\text{Ire}}(t) = 1$  and  $\tilde{\mathcal{L}}_{\text{Ire}}^{(k)}(t)$  is obtained in a recursive way, as follows

$$\tilde{\mathcal{L}}_{\text{Ire}}^{(k)}(t) = \sum_{l=0}^{k-1} \binom{k-1}{l} \tilde{\eta}^{(k-l)}(t) \times \tilde{\mathcal{L}}_{\text{Ire}}^{(l)}(t), \quad k > 0, \quad (46)$$

where

$$\tilde{\eta}^{(k)}(t) = (-1)^k 2\pi\lambda \left[ \mu_b^k \Gamma(1 + k) \int_t^\infty (\ell_b(r))^{-k\alpha_N} r dr + 2p \times \sum_{i \in \{L, N\}} \frac{\Gamma(m_i + k) \mu_u^k}{\Gamma(m_i) m_i^k} \int_0^\infty \mathcal{G}^k(r) (r^2 + h^2)^{-\frac{k\alpha_i}{2}} P_i(r) r dr \right]. \quad (47)$$

*Proof:* See Appendix C.

To sum up, Tab. I provides the diversity gain and the constant term  $\varrho$  for different modes of cooperation, and the power gain is easily obtained via (40).

#### D. Normalized Spectral Efficiency

In order to evaluate the impact of the coordinated transmission on the overall network performance, the normalized spectral efficiency (NSE) is considered and defined by

$$\text{NSE} \triangleq \frac{1 - \varpi}{\mathcal{N}} \mathbb{E} \left[ \ln(1 + \text{SIR}) \right], \quad (48)$$

where  $\varpi \in [0, 1]$  denotes the time fraction of exchanging the control signals and data among the coordinated points, and the denominator  $\mathcal{N}$  is the total number of the points participating in the coordination. Specifically,  $\mathcal{N} = N + 1$  for the case with UAV assistance while  $\mathcal{N} = N$  for the case without UAV assistance. For BSS, the signaling overhead can be neglected compared with JT, hence  $\varpi = 0$  in this option.

**Theorem 4.** *The NSE of the worst-case user is approximated as*

$$\text{NSE} \approx \int_0^\infty \int_0^\infty \frac{f_D(t)}{\mathcal{N}} \sum_{n=1}^K \binom{K}{n} \frac{(-1)^{n+1}}{\varepsilon + 1} \mathcal{L}_I\left(\frac{n\xi\varepsilon}{\theta}, t\right) d\varepsilon dt. \quad (49)$$

*Proof:* According to the definition of the NSE, we have

$$\begin{aligned} & \mathbb{E} \left[ \ln \left( 1 + \frac{S}{I} \right) \right] \\ &= \int_0^\infty \int_0^\infty \mathbb{P} \left( \ln \left( 1 + \frac{S}{I} \right) > v \right) dv f_D(t) dt \\ &\stackrel{(a)}{=} \int_0^\infty \int_0^\infty \frac{1}{\varepsilon + 1} \mathbb{P}(S > \varepsilon I) d\varepsilon f_D(t) dt \\ &\stackrel{(b)}{\approx} \int_0^\infty \int_0^\infty \sum_{n=1}^K \binom{K}{n} \frac{(-1)^{n+1} f_D(t)}{\varepsilon + 1} \mathcal{L}_I\left(\frac{n\xi\varepsilon}{\theta(t)}, t\right) d\varepsilon dt, \quad (50) \end{aligned}$$

where step (a) is obtained by replacing  $e^v - 1$  with  $\varepsilon$  and step (b) is similar to the derivation of the success probability. ■

## IV. NUMERICAL RESULTS

In this section, we give numerical results of the performance evaluation for the worst-case users via the proposed flexible and general air-ground cooperation scheme, where the main coordinated manners include BSS and JT, each of which has 7 options corresponding to  $N = 0, 1, 2, 3$  with UAV assistance and  $N = 1, 2, 3$  without UAV assistance. The main symbols

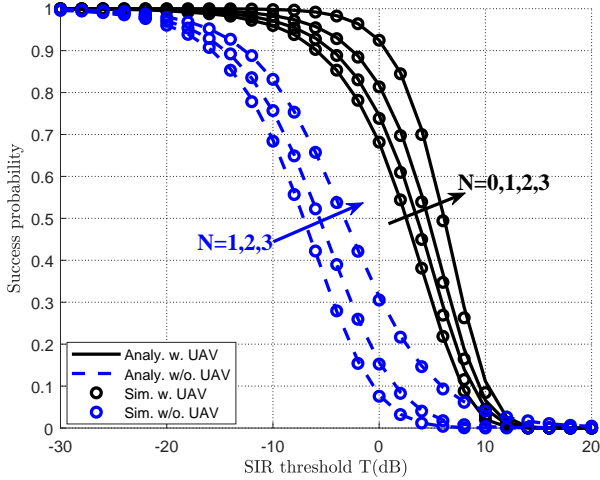


Fig. 2. The success probabilities for BSS-based air-ground cooperations.

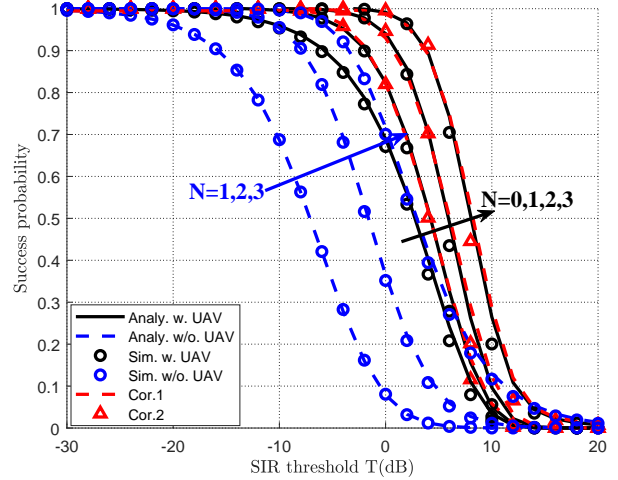


Fig. 3. The success probabilities for JT-based air-ground cooperations.

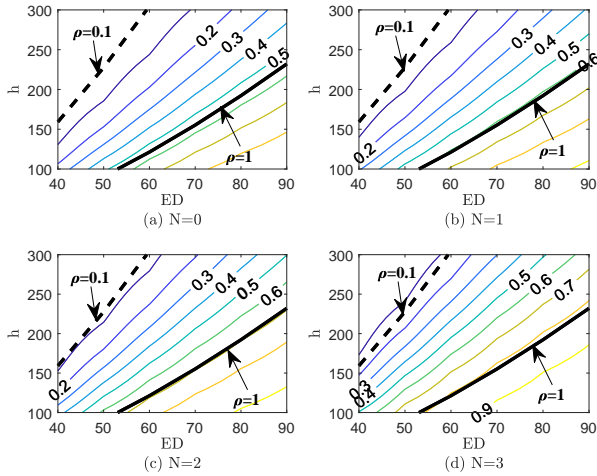


Fig. 4. Contour plots of success probability for BSS-based air-ground cooperations.

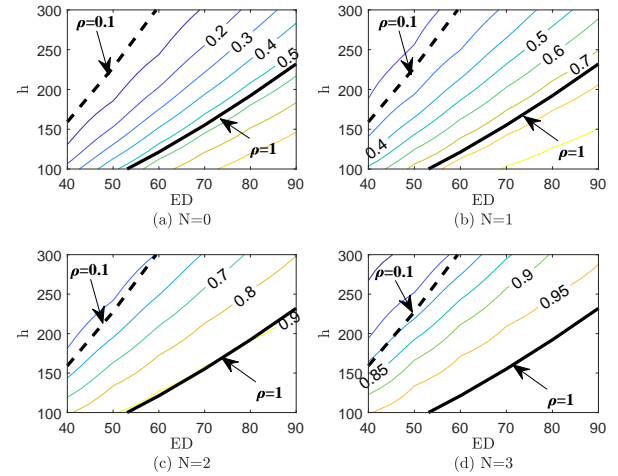


Fig. 5. Contour plots of success probability for JT-based air-ground cooperations.

and parameters are summarized in Tab. II, and the default values are given where applicable.

Fig. 2 and Fig. 3 show the success probabilities for BSS- and JT-based air-ground cooperations with and without UAV assistance, respectively. It can be seen that the analytical results match the simulations well, validating the accuracy of Thms. 1-2 and Cors. 1-2. For the given system parameters, the performance of the cooperation with UAV is significantly better than that without UAV and the performance gain brought by the UAV in BSS-based cooperation is higher than that in JT-based cooperation. It should be noted that the results with  $N = 0$  in both figures are the same, corresponding to the case served by single UAV, which could be regarded as benchmarks compared with the multi-point coordination cases. Besides, the performance in both BSS-based and JT-based air-ground cooperations increases with  $N$ , i.e., the number of coordinated points due to the advantages of CoMP that eliminates the main interferers while increasing or maintaining the desired signal strength.

In Fig. 4 and Fig. 5, we plot the contour of the success

probability in BSS- and JT-based air-ground cooperation as a function of  $\mathbb{E}D$  and  $h$  for different  $N$ , where  $T = 0$  dB, and also add two curves with  $\rho = 1$  and  $\rho = 0.1$  on each plot, where  $\rho$  represents the UBPR, defined in (4). It can be observed that the two curves are roughly parallel to the contour curves with a fixed success probability in all cases, especially for  $\rho = 1$ , which means that as long as  $\rho$  is given, the performance of the worst-case user is roughly determined. For  $\rho = 0.1$ , the received signal strength from the nearest BSs is much stronger than the serving UAV and hence becomes the dominant factor in affecting the worst-case user's performance. In this regard, the randomness of  $D$  makes the ratio  $\rho$  based on the average power deviate from that based on the instantaneous power, causing the curve with  $\rho = 0.1$  not as parallel as that with  $\rho = 1$ . Furthermore, as  $\rho$  increases, namely, as  $h$  decreases or  $\mathbb{E}D$  increases, the success probability is improved for all cases due to the strengthened desired signal from the UAV and the reduced interfering signal from the nearest BSs. In short, the two figures demonstrate how the critical parameter  $\rho$  dominates the performance of the proposed air-

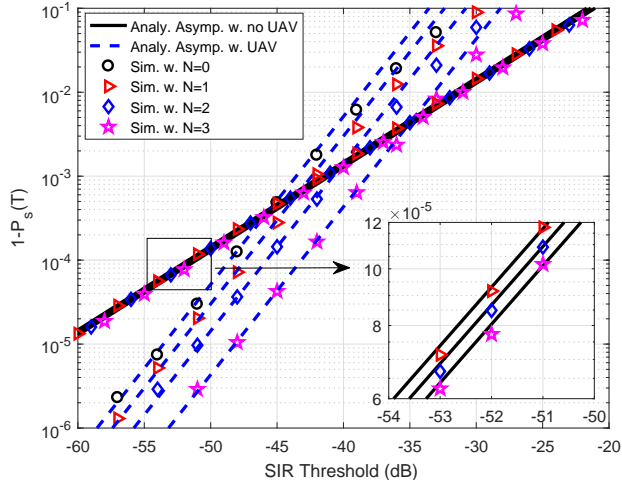


Fig. 6. The asymptotic outage probabilities for different BSS-based cooperation schemes.

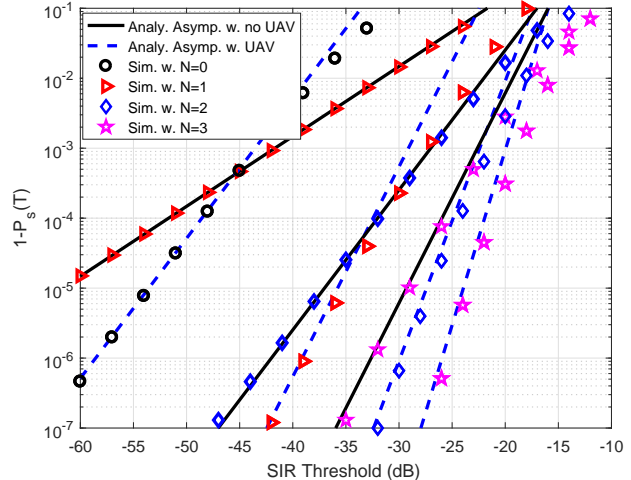


Fig. 7. The asymptotic outage probabilities for different JT-based cooperation schemes.

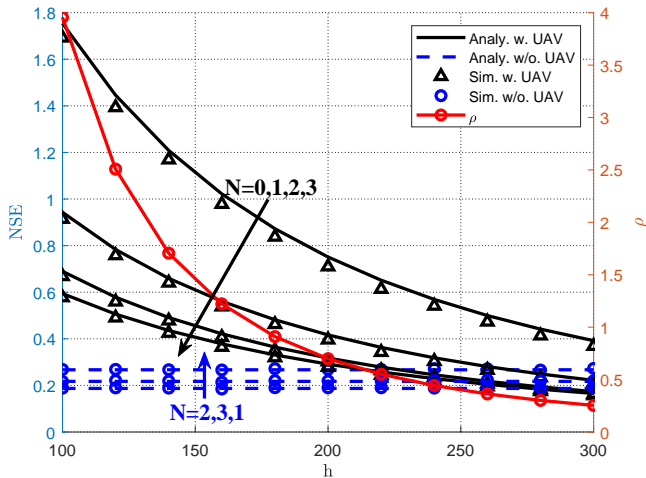


Fig. 8. The NSE and UBPR  $\rho$  for BSS-based air-ground cooperations.

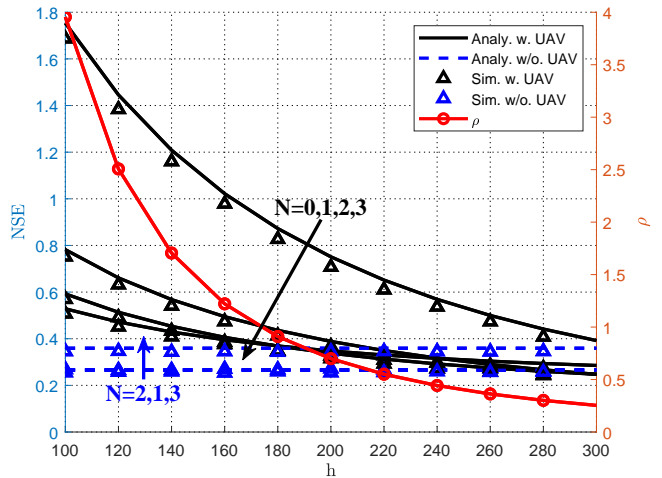


Fig. 9. The NSE and UBPR  $\rho$  for JT-based air-ground cooperations.

ground cooperation scheme and guides us to adjust the manner of cooperation to specific scenario configurations flexibly.

Fig. 6 and Fig. 7 show the asymptotic behavior of the outage probability as  $T \rightarrow 0$  for BSS- and JT-based air-ground cooperations with and without UAV assistance, respectively, where  $m_L = 2$ ,  $h = 200\text{m}$ ,  $\lambda = 0.001\text{m}^{-2}$ ,  $p = 1$ ,  $G_m = 5$ ,  $G_s = 1$  and  $\psi_m = 5^\circ$ . In both figures, it is shown that the simulations are close to the analytical asymptote when  $T \rightarrow 0$ , which demonstrates the correctness of Thm. 3. The asymptotic slope of  $\log(1 - P_s(T))$  w.r.t.  $T$  in dB is the diversity gain, which is independent of  $N$  in BSS-based cooperations in Fig. 6 and increases linearly with  $N$  in JT-based cooperations in Fig. 7. In addition, the slope of the cases with UAV assistance is larger than that without UAV assistance due to the better fading conditions of air-to-ground LOS channel. The horizontal gap between the two curves with the same slope is the power gain, and we can see that it increases with  $N$  in all cases. For BSS-based cooperations, relative to the case of  $N = 0$  where no BS is silenced, the power gain for  $N > 0$  with UAV assistance is much larger than the case without UAV assistance. This

is because in the current parameter setting,  $\rho = 0.07$  which means the average signal strength from a nearest BS is much higher than that from the UAV. Thus, when the user is served by a UAV, silencing a strong interfering BS will yield a visible power gain, while the power gain could be negligible when the user is served by a BS. In contrast, the asymptote of JT-based cooperation has a faster decay rate to zero (i.e., bigger diversity) and yields a bigger horizontal gap for the same curve slope (i.e., higher power gain), which highlights the significant performance enhancement of JT-based air-ground cooperation in the high-reliability regime.

Fig. 8 and Fig. 9 demonstrate the NSE and the UBPR ratio  $\rho$  versus the UAV's height  $h$  for BSS- and JT-based air-ground cooperations with and without UAV assistance, respectively. The alignment between the analytical and simulation results affirms the accuracy of Thm. 4. As  $h$  increases, the NSE of the cases with UAV assistance and  $\rho$  gradually decrease due to the signal attenuation from the UAV. Interestingly, it is found that either with or without UAV assistance, the NSE for the case of single serving point is higher than the multi-point cases,

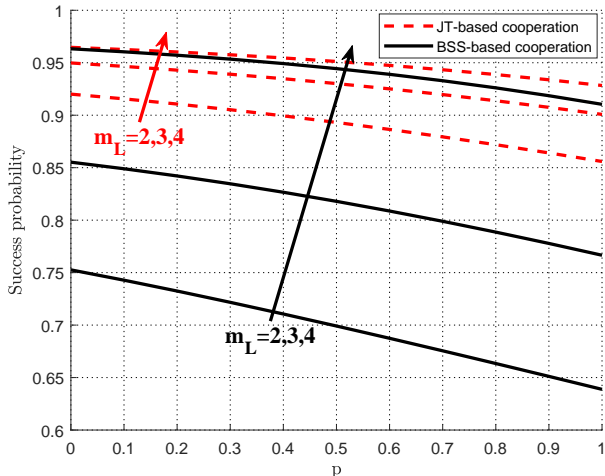


Fig. 10. The comparison of success probabilities for different air-ground cooperations with UAV assistance.

which is just opposite in terms of the success probability. This indicates that improving the worst-case user's performance by single point (especially the UAV) would be more cost-effective than multiple points from the perspective of spectral efficiency. Moreover, with the increase of  $N$ , the NSE of JT-based cooperations with UAV assistance deteriorates even faster than that of BSS-based cooperations due to the extra cost of data exchange. From the relationship between  $\rho$  and the performance improvement by introducing the UAV, we can find that when  $\rho \gg 1$ , whether using a single UAV or the air-ground cooperation to help improve the worst-case user's performance is significantly superior to that served by pure ground BSs, but such superiority would gradually decrease with the decrease of  $\rho$ .

Fig. 10 shows how the success probabilities of BSS- and JT-based air-ground cooperations change with the density of UAVs reflected by parameter  $p$  and fading parameter  $m_L$  for  $N = 1$  and  $T = 0$  dB. It can be seen that the success probability decreases with the increase of  $p$  since more UAVs deployed, more severe interference caused. Furthermore, a larger  $m_L$  leads to a higher success probability due to the better air-to-ground channel fading condition for all cooperation schemes. For the same  $m_L$ , the JT-based cooperation is always better than the BSS-based one, and the performance gap between the two schemes becomes smaller as  $m_L$  increases. This is because in the BSS-based cooperation, the desired signal merely comes from the UAV while in the JT-based cooperation, it also has an extra copy from a nearest BS contributing to the performance gain. However, if the air-to-ground channel condition is obviously superior to the ground channel, e.g., a larger  $m_L$ , the UAV's signal would probably dominate the received desired signal strength of the worst-case user, e.g.,  $\rho \approx 14 \gg 1$  under the default parameter setting. In this case, the contribution from a nearest BS in JT-based cooperation becomes negligible.

Fig. 11 compares the BSS- and JT-based cooperation schemes in terms of NSE versus the time fraction  $\varpi$  for exchanging the signaling overhead and data with different

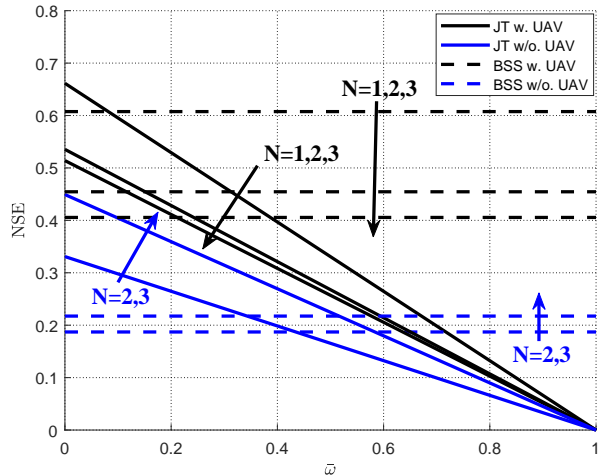


Fig. 11. The comparison of NSE for different air-ground cooperations.

$N$ . It is seen that as  $N$  increases, the NSE for the two cooperation schemes with UAV assistance becomes worse while the opposite phenomena occurs in the case without UAV assistance, which is consistent with the results in Fig. 8 and Fig. 9. Moreover, as  $\varpi$  increases, the NSEs of JT-based cooperations are all linearly decreased while unchanged in BSS-based cooperations, which obviously demonstrates the impact of the cost for data exchange on the NSE of each cooperation scheme. For each case of  $N$ , the crossover point between the JT and BSS curves shows at what value of  $\varpi$  the BSS becomes more efficient. To be specific, at the beginning stage of increasing  $\varpi$ , the NSE of JT-based scheme is superior to BSS-based scheme and the larger the number of coordinated BSs, the wider the range of  $\varpi$  maintaining such superiority. This indicates that the negative effects of data exchange and signaling overhead can be offset by increasing the number of coordinated BSs. However, as  $\varpi$  continues to increase, the benefits of JT are increasingly unable to compensate for the cost, making the NSE significantly less than that of BSS.

## V. CONCLUSION

In this paper, a flexible air-ground cooperation scheme was proposed for improving the performance of cell-corner users in a Poisson cellular network, which stands out for the UAV's adaptability and allows for different levels of cooperation. To fully evaluate the benefits brought by this scheme, we derived the success probability and cooperation gain for the worst-case user under BSS- and JT-based air-ground cooperations with and without UAV assistance, respectively. Results showed that the air-ground cooperation outperforms the pure ground cooperation by a landslide in terms of the user-perceived performance, and the more the coordinated points, the better the performance. Furthermore, we also analyzed the normalized spectral efficiency to characterize the cost of each type of cooperation. It is concluded that improving the worst-case user's performance by single point (especially the UAV) is more cost-effective than multiple points from the perspective of spectral efficiency (network-level performance),

which is exactly different from the conclusions obtained from the success probability (link-level performance). This tells us that both the network- and link-level performance should be taken into account when choosing the manner of cooperation and coordinated points. Additionally, the UBPR  $\rho$  is a key parameter that determines the necessity of introducing the UAV into the cooperation and the gain that can be obtained.

#### APPENDIX A PROOF OF LEMMA 1

*Proof:* According to Eq. (6), The Laplace transform of the interference from non-cooperative BSs is given by

$$\begin{aligned} \mathcal{L}_{I_{nc}}(s, t) &= \mathbb{E} \left[ \prod_{y \in \mathcal{V} \setminus \mathcal{W}} e^{-s\mu_b g_y \ell_b(D)} \mid D = t \right] \\ &= \left( \frac{1}{1 + \mu_b s \ell_b(t)} \right)^{3-N}. \end{aligned} \quad (51)$$

Combining the two cases, we obtain a unified expression for  $\mathcal{L}_{I_{nc}}(s, t)$  in Lemma 1.

For the interference from other BSs in  $\Phi_b \setminus \mathcal{V}$ , we have

$$\begin{aligned} \mathcal{L}_{I_b}(s, t) &= \mathbb{E} \left[ \prod_{x \in \Phi \setminus \mathcal{V}} e^{-s\mu_b g_x \ell_b(\|x\|)} \mid D = t \right] \\ &\stackrel{(a)}{=} \exp \left( -2\pi\lambda \int_t^\infty \left( 1 - \mathbb{E}[\exp(-s\mu_b g_x \ell_b(r))] \right) r dr \right) \\ &= \exp \left( -2\pi\lambda \int_t^\infty \frac{r}{1 + \mu_b^{-1} s^{-1} \ell_b^{-1}(r)} dr \right) \end{aligned} \quad (52)$$

where step (a) follows from the probability generating functional (PGFL) of the PPP [32].

For the interference from UAVs in  $\Phi_u$ , if there is no UAV hovering over the typical worst-case user, we have

$$\begin{aligned} \mathcal{L}_{I_u}(s) &= \mathbb{E} \left[ \prod_{x \in \Phi_u} \sum_{i \in \{L, N\}} \frac{P_i(\|x\|)}{\left( 1 + \frac{sG_x \mu_u}{m_i(\|x\|^2 + h^2)^{\alpha_i/2}} \right)^{m_i}} \right] \\ &\stackrel{(b)}{\approx} \mathbb{E} \left[ \prod_{x \in \Phi_{PPP}} \sum_{i \in \{L, N\}} \frac{P_i(\|x\|)}{\left( 1 + \frac{sG_x \mu_u}{m_i(\|x\|^2 + h^2)^{\alpha_i/2}} \right)^{m_i}} \right] \\ &= \exp \left( -2p\lambda \int_{\mathbb{R}^2} 1 - \sum_{i \in \{L, N\}} \frac{P_i(\|x\|)}{\left( 1 + \frac{sG_x \mu_u}{m_i(\|x\|^2 + h^2)^{\alpha_i/2}} \right)^{m_i}} dx \right) \\ &= \exp \left( -4\pi p\lambda \sum_{i \in \{L, N\}} \left( \int_0^{R_m} \left( 1 - \frac{1}{\left( 1 + \frac{sG_m \mu_u}{m_i(r^2 + h^2)^{\alpha_i/2}} \right)^{m_i}} \right) \right. \right. \\ &\quad \left. \left. \times P_i(r) r dr + \int_{R_m}^\infty \left( 1 - \frac{1}{\left( 1 + \frac{sG_s \mu_u}{m_i(r^2 + h^2)^{\alpha_i/2}} \right)^{m_i}} \right) P_i(r) r dr \right) \right) \\ &= \exp \left( -4p\pi\lambda \sum_{i \in \{L, N\}} \int_0^\infty \Psi_i(s, r, \mathcal{G}(r)) P_i(r) r dr \right), \end{aligned} \quad (53)$$

where in step (b) a homogeneous PPP  $\Phi_{PPP}$  with the same density  $2p\lambda$  is adopted to approximate the UAV point process  $\Phi_u$ . If there is a UAV participating in the air-ground cooperation, the interference other UAVs in  $\Phi_u \setminus \{u_0\}$  has the same expression of the Laplace transform as in (53) using the PPP approximation due to the Slivnyak's theorem [32]. ■

#### APPENDIX B PROOF OF LEMMA 2

*Proof:* Through the formula of Leibniz, we can derive the  $n$ -th derivative of  $\mathcal{L}_I(s, t)$  w.r.t.  $s$  as

$$\mathcal{L}_I^{(n)}(s, t) = \sum_{k=0}^n \binom{n}{k} \mathcal{L}_{I_{nc}}^{(n-k)}(s, t) \mathcal{L}_{I_{re}}^{(k)}(s, t). \quad (54)$$

It is easy to obtain the expression of  $\mathcal{L}_{I_{nc}}^{(k)}(s, t)$ ,  $k = 1, \dots, n$  through the chain rule of the derivatives.

For  $\mathcal{L}_{I_{re}}(s, t)$ , we can observe that  $\mathcal{L}_{I_{re}}^{(1)}(s, t) = \eta'(s, t) \mathcal{L}_{I_{re}}(s, t)$ , thus according to the formula of Leibniz, we can calculate  $\mathcal{L}_{I_{re}}^{(n)}(s, t)$  recursively as

$$\mathcal{L}_{I_{re}}^{(n)}(s, t) = \sum_{k=0}^{n-1} \binom{n-1}{k} \eta^{(n-k)}(s, t) \mathcal{L}_{I_{re}}^{(k)}(s, t), \quad (55)$$

where the  $k$ -th order derivative of  $\eta(s, t)$  w.r.t.  $s$  is obtained in a straightforward way. Using  $\Psi_i(s, r, x)$  and  $\mathcal{G}(r)$ , the final result is obtained. ■

#### APPENDIX C PROOF OF THEOREM 3

*Proof:* Similar to the derivation of the success probability, we first analyze the cases of BSS with/without UAV assistance and JT without UAV assistance, in which the scaling parameter of the gamma variable  $S$  is integer. Thus, the outage probability is given by

$$\begin{aligned} 1 - P_s(T) &= \mathbb{P}(S < TI) \\ &= \int_0^\infty \mathbb{E} \left[ \tilde{\gamma} \left( K, \frac{TI(t)}{\theta(t)} \mid D = t \right) f_D(t) dt \right] \\ &\stackrel{(a)}{\approx} T^K \int_0^\infty \frac{\mathbb{E}[I(t) \mid D = t]^K}{\Gamma(K+1) [\theta(t)]^K} f_D(t) dt, \quad T \rightarrow 0 \\ &\stackrel{(b)}{\approx} T^K \int_0^\infty \frac{(-1)^K \mathcal{L}_I^{(K)}(s, t)|_{s=0}}{\Gamma(K+1) [\theta(t)]^K} f_D(t) dt, \quad T \rightarrow 0, \end{aligned} \quad (56)$$

where step (a) is obtained using the asymptotic behavior of the normalized lower incomplete gamma function  $\tilde{\gamma}(k, x) \sim \frac{x^k}{\Gamma(k+1)}$ ,  $x \rightarrow 0$ , and step (b) follows from  $\mathbb{E}I^k = (-1)^k \mathcal{L}_I^{(k)}(s)|_{s=0}$ . In these cases, the diversity gain  $d$  is equal to the scaling parameter  $K$  of the gamma variable  $S$ , shown in Tab. I.

Next, we analyze the case of JT with UAV assistance, where the desired signal power is the sum of two gamma random variables with the scaling parameters  $m_L$  and  $N$  as well as the shape parameters  $\frac{\mu_u G_m h^{-\alpha_L}}{m_L}$  and  $\mu_b \ell_b(t)$ , respectively. According to the results in [28], the exact PDF of  $S$  is

$$f_S(y) = C \sum_{i=0}^\infty \frac{c_i y^{K+i-1} \exp\left(-\frac{y}{\theta_{\min}}\right)}{\Gamma(K+i) \theta_{\min}^{K+i}}, \quad (57)$$

where  $K = m_L + N$ ,  $\theta_{\min} = \min\left(\frac{\mu_u G_m h^{-\alpha_L}}{m_L}, \mu_b \ell_b(t)\right)$ ,  $C = \theta_{\min}^K \left(\frac{m_L h^{\alpha_L}}{\mu_u G_m}\right)^{m_L} (\mu_b \ell_b(t))^{-N}$  and  $c_0 = 1$ .

$$\begin{aligned} 1 - P_s(T) &= \mathbb{P}(S < TI) \\ &= \int_0^\infty \mathbb{E}_I \left[ \int_0^{TI} C \sum_{i=0}^\infty \frac{c_i y^{K+i-1} \exp\left(-\frac{y}{\theta_{\min}}\right)}{\Gamma(K+i) \theta_{\min}^{K+i}} dy \right] f_D(t) dt \end{aligned}$$

$$\begin{aligned}
&= \int_0^\infty \mathbb{E}_I \left[ C \sum_{i=0}^\infty c_i \tilde{\gamma}(K+i, TI/\theta_{\min}) \right] f_D(t) dt \\
&\sim \int_0^\infty \mathbb{E}_I \left[ C \sum_{i=0}^\infty c_i \frac{(TI/\theta_{\min})^{K+i}}{\Gamma(K+i+1)} \right] f_D(t) dt, T \rightarrow 0 \\
&\sim \int_0^\infty \mathbb{E}_I \left[ C c_0 \frac{(TI/\theta_{\min})^K}{\Gamma(K+1)} \right] f_D(t) dt, T \rightarrow 0 \\
&\sim T^K \int_0^\infty \frac{(\frac{m_L h^{\alpha_L}}{\mu_u G_m})^{m_L} (\mu_b \ell_b(t))^{-N}}{\Gamma(K+1)} \mathbb{E}_I [I^K] f_D(t) dt, T \rightarrow 0 \\
&\sim T^K \int_0^\infty \frac{(-1)^K \mathcal{L}_I^{(K)}(s, t)|_{s=0} f_D(t) dt}{\Gamma(K+1) (\frac{\mu_u G_m h^{\alpha_L}}{m_L})^{m_L} (\mu_b \ell_b(t))^N}, T \rightarrow 0. \quad (58)
\end{aligned}$$

In this case, the diversity gain  $d$  is  $N + m_L$ , which is equal to the sum of the number of coordinated BSs  $N$  and the Nakagami parameter  $m_L$ . ■

## REFERENCES

- [1] R. Wu, N. Deng, M. Haenggi, H. Wei, and N. Zhao, "Performance analysis of cellular edge users with air-ground cooperation," in *2024 IEEE Wireless Communications and Networking Conference (WCNC)*, Dubai, United Arab Emirates, April 2024, pp. 1–6.
- [2] M. S. Ibrahim, A. S. Zamzam, A. Konar, and N. D. Sidiropoulos, "Cell-edge detection via selective cooperation and generalized canonical correlation," *IEEE Transactions on Wireless Communications*, vol. 20, no. 11, pp. 7431–7444, Nov. 2021.
- [3] J. Qi, N. Deng, and H. Wei, "Success probability of Gauss-Poisson UAV-assisted cellular networks with mobility," in *2023 IEEE International Conference on Communications Workshops (ICC Workshops)*, Rome, Italy, May 2023, pp. 1914–1919.
- [4] J. Zheng, Z. Wang, and A. Jamalipour, "An aerial and ground base station cooperation strategy for uav and cellular integrated networks," *IEEE Internet of Things Journal*, vol. 11, no. 6, pp. 10411–10424, March 2024.
- [5] M. Hui, J. Chen, L. Yang, L. Lv, H. Jiang, and N. Al-Dhahir, "UAV-assisted mobile edge computing: Optimal design of UAV altitude and task offloading," *IEEE Transactions on Wireless Communications*, 2024, IEEE Early Access.
- [6] E. Dahlman, S. Parkvall, and J. Skold, *5G NR: The next generation wireless access technology*. Academic Press, 2020.
- [7] X. Zhang and M. Haenggi, "A stochastic geometry analysis of inter-cell interference coordination and intra-cell diversity," *IEEE Transactions on Wireless Communications*, vol. 13, no. 12, pp. 6655–6669, Dec. 2014.
- [8] H. Wei, N. Deng, and M. Haenggi, "Performance analysis of inter-cell interference coordination in mm-wave cellular networks," *IEEE Transactions on Wireless Communications*, vol. 21, no. 2, pp. 726–738, Feb. 2022.
- [9] G. Zhao, S. Chen, L. Zhao, and L. Hanzo, "Joint energy-spectral-efficiency optimization of CoMP and BS deployment in dense large-scale cellular networks," *IEEE Transactions on Wireless Communications*, vol. 16, no. 7, pp. 4832–4847, July 2017.
- [10] M. Elhatab, M. A. Arfaoui, and C. Assi, "A joint CoMP C-NOMA for enhanced cellular system performance," *IEEE Communications Letters*, vol. 24, no. 9, pp. 1919–1923, Sept. 2020.
- [11] Y. Sun, Z. Ding, X. Dai, M. Zhou, and Z. Ding, "Stochastic geometry based modeling and analysis on network NOMA in downlink CoMP systems," *IEEE Transactions on Vehicular Technology*, vol. 73, no. 1, pp. 1388–1393, Jan. 2024.
- [12] S. Y. Jung, H.-k. Lee, and S.-L. Kim, "Worst-case user analysis in Poisson Voronoi cells," *IEEE Communications Letters*, vol. 17, no. 8, pp. 1580–1583, Aug. 2013.
- [13] G. Nigam, P. Minero, and M. Haenggi, "Coordinated multipoint joint transmission in heterogeneous networks," *IEEE Transactions on Communications*, vol. 62, no. 11, pp. 4134–4146, Nov. 2014.
- [14] Q. Cui, X. Yu, Y. Wang, and M. Haenggi, "The SIR meta distribution in Poisson cellular networks with base station cooperation," *IEEE Transactions on Communications*, vol. 66, no. 3, pp. 1234–1249, March 2018.
- [15] A. Fotouhi, H. Qiang, M. Ding, M. Hassan, L. G. Giordano, A. Garcia-Rodriguez, and J. Yuan, "Survey on UAV cellular communications: Practical aspects, standardization advancements, regulation, and security challenges," *IEEE Communications Surveys & Tutorials*, vol. 21, no. 4, pp. 3417–3442, Fourth quarter 2019.
- [16] M. Matracia, M. A. Kishk, and M.-S. Alouini, "Coverage analysis for UAV-assisted cellular networks in rural areas," *IEEE Open Journal of Vehicular Technology*, vol. 2, pp. 194–206, April 2021.
- [17] —, "UAV-aided post-disaster cellular networks: A novel stochastic geometry approach," *IEEE Transactions on Vehicular Technology*, vol. 72, no. 7, pp. 9406–9418, July 2023.
- [18] O. M. Bushnaq, M. A. Kishk, A. Celik, M.-S. Alouini, and T. Y. Al-Naffouri, "Optimal deployment of tethered drones for maximum cellular coverage in user clusters," *IEEE Transactions on Wireless Communications*, vol. 20, no. 3, pp. 2092–2108, March 2021.
- [19] H. Wu, Z. Wei, Y. Hou, N. Zhang, and X. Tao, "Cell-edge user offloading via flying UAV in non-uniform heterogeneous cellular networks," *IEEE Transactions on Wireless Communications*, vol. 19, no. 4, pp. 2411–2426, April 2020.
- [20] N. Deng, H. Wei, and M. Haenggi, "Modeling and analysis of air-ground integrated networks with flexible beam coverage," *IEEE Transactions on Wireless Communications*, vol. 22, no. 11, pp. 8170–8184, Nov. 2023.
- [21] Y. Sun, Z. Ding, and X. Dai, "A user-centric cooperative scheme for uav-assisted wireless networks in malfunction areas," *IEEE Transactions on Communications*, vol. 67, no. 12, pp. 8786–8800, Dec. 2019.
- [22] K. Feng and M. Haenggi, "A location-dependent base station cooperation scheme for cellular networks," *IEEE Transactions on Communications*, vol. 67, no. 9, pp. 6415–6426, Sept. 2019.
- [23] M. Haenggi, "A versatile dependent model for heterogeneous cellular networks," *CoRR*, vol. abs/1305.0947, 2013. [Online]. Available: <http://arxiv.org/abs/1305.0947>
- [24] X. Shi and N. Deng, "Modeling and analysis of mmwave UAV swarm networks: A stochastic geometry approach," *IEEE Transactions on Wireless Communications*, vol. 21, no. 11, pp. 9447–9459, Nov. 2022.
- [25] A. Al-Hourani, S. Kandeepan, and S. Lardner, "Optimal LAP altitude for maximum coverage," *IEEE Wireless Communications Letters*, vol. 3, no. 6, pp. 569–572, Dec. 2014.
- [26] R. Tanbourgi, S. Singh, J. G. Andrews, and F. K. Jondral, "A tractable model for noncoherent joint-transmission base station cooperation," *IEEE Transactions on Wireless Communications*, vol. 13, no. 9, pp. 4959–4973, Sept. 2014.
- [27] J. G. Andrews, F. Baccelli, and R. K. Ganti, "A tractable approach to coverage and rate in cellular networks," *IEEE Transactions on Communications*, vol. 59, no. 11, pp. 3122–3134, Nov. 2011.
- [28] P. G. Moschopoulos, "The distribution of the sum of independent gamma random variables," *Annals of the Institute of Statistical Mathematics*, vol. 37, no. 1, pp. 541–544, 1985.
- [29] R. W. Heath Jr, T. Wu, Y. H. Kwon, and A. C. K. Soong, "Multiuser mimo in distributed antenna systems with out-of-cell interference," *IEEE Transactions on Signal Processing*, vol. 59, no. 10, pp. 4885–4899, Oct. 2011.
- [30] H. Alzer, "On some inequalities for the incomplete gamma function," *Mathematics of Computation*, vol. 66, no. 218, pp. 771–778, 1997.
- [31] X. Wang, H. Zhang, Y. Tian, and V. C. M. Leung, "Modeling and analysis of aerial base station-assisted cellular networks in finite areas under LoS and NLoS propagation," *IEEE Transactions on Wireless Communications*, vol. 17, no. 10, pp. 6985–7000, Oct. 2018.
- [32] M. Haenggi, *Stochastic geometry for wireless networks*. Cambridge University Press, 2012.